Molten Salt Synthesis and Properties of Three New Solid-State Ternary Bismuth Chalcogenides, β-$CsBiS_2$, γ-$CsBiS_2$, and $K_2Bi_8Se_{13}$

Timothy J. McCarthy,[†] Stanley-Pierre Ngeyi,[†,‡] Ju-Hsiou Liao,[†] Donald C. DeGroot,[§] Tim Hogan,[§] Carl R. Kannewurf,[§] and Mercouri G. Kanatzidis*[,†,⊥]

Department of Chemistry and Center for Fundamental Materials Research, Michigan State University, East Lansing, Michigan 48824, and Department of Electrical Engineering and Computer Science, Northwestern University, Evanston, Illinois 60208

Received October 14, 1992. Revised Manuscript Received December 17, 1992

β-$CsBiS_2$, γ-$CsBiS_2$, and $K_2Bi_8Se_{13}$ were synthesized by the alkali metal polychalcogenide flux technique. An investigation of the Bi/Cs_2S_x system at 290 °C revealed the presence of a new ternary sulfide β-$CsBiS_2$ (I) (83% yield). The red substance crystallizes in the monoclinic $P2_1/c$ space group (No. 14) with a = 7.794(5) Å, b = 9.610(6) Å, c = 7.329(4) Å, β = 102.16(5)°. The final R/R_w = 7.4/10%. The structure consists of BiS_3 trigonal pyramids connected at two vertices to form $(BiS_2)_n^{n-}$ chains along the a axis with Cs^+ ions in between the chains. β-$CsBiS_2$ is an insulator. γ-$CsBiS_2$ was obtained as above but at 350 °C. It crystallizes in the rhombohedral system with a = 4.166(4) Å and c = 48.77(5) Å. It has a superstructure related to that of $RbBiS_2$. Similar investigations in the Bi/K_2Se_x system at 330 °C gave the new ternary selenide $K_2Bi_8Se_{13}$ (II) (88% yield). This compound crystallizes in the triclinic $P\bar{1}$ space group (No. 2) with a = 13.768(2) Å, b = 12.093(3) Å, c = 4.1656(6) Å, α = 89.98(1)°, β = 98.64(1)°, γ = 87.96(1)°. The final R/R_w = 8.2/8.9%. The structure of the black crystals consists of layers of $BiSe_6$ octahedra with $BiSe_5$ square pyramidal units connecting the layers to form a three-dimensional network with K^+ ions located in the channels. The $[Bi_8Se_{13}]^{2-}$ framework can be thought of as a hybrid of three different layered structure types interconnected to form a 3-D network. Structural features from the Bi_2Te_3, Sb_2S_3, and CdI_2 lattices are represented in this framework. Electrical conductivity and thermopower measurements on γ-$CsBiS_2$ and $K_2Bi_8Se_{13}$ show n-type semiconducting behavior. For both materials the room temperature conductivity is $\sim 10^{-2}$ S/cm. The reaction of Bi with Cs_2S_x and K_2Se_x fluxes was investigated with differential scanning calorimetry (DSC). The optical band gaps of β-$CsBiS_2$, γ-$CsBiS_2$, and $K_2Bi_8Se_{13}$ were determined by UV/vis/near-IR diffuse reflectance measurements to be 1.43, 1.11, and 0.76 eV, respectively.

Introduction

To date, there are only a few structurally characterized ternary alkali metal bismuth chalcogenides, outside of the well-known NaCl-type $ABiQ_2$ (A = Li, Na, K; Q = S, Se, Te) compounds.[1,2] To the best of our knowledge, the only other structurally characterized phases are $CsBi_3S_5$,[3] $RbBi_3S_5$,[4] $Cs_3Bi_7Se_{12}$,[5] and $Sr_4Bi_6Se_{13}$.[6] This relative scarcity of ternary compounds provides a further impetus for exploratory research in this area. In particular, Bi is very attractive for study because of its $6s^2$ lone pair of electrons which may or may not be manifested structurally in a given compound. Whether the lone pair is stereochemically active or not affects both the lattice structure and the properties of the resulting compounds and thus exploration of the solid state chemistry of Bi is warranted. This issue is related to the larger question of stereochemical activity of a lone pair in compounds with elements in a s^2 configuration.

Group 15 chalcogenide compounds have received considerable attention, due to their potential application as nonlinear optical materials,[7] photoelectrics,[8] and thermoelectrics.[9] The most common application that is unique to group 15 chalcogenides is in the area of thermoelectric cooling materials. To date, the most investigated systems are various solid solutions of M_2Q_3 (M = As, Sb, Bi; Q = S, Se, Te) compounds.[10] These materials possess high electrical conductivity and thermoelectric power and low

† Michigan State University.
‡ PRF Summer Fellow, Department of Chemistry, Madonna University, Livonia, Michigan 48150.
§ Northwestern University.
⊥ A. P. Sloan Foundation Fellow, 1991-1993.

(1) (a) Boon, J. W. *Recl. Trav. Chim. Pays-Bas* **1944**, *63*, 32. (b) Glemser, O.; Filcek, M. *Z. Anorg. Allg. Chem.* **1955**, *279*, 321-323. (c) Gattow, G.; Zemann, J. *Z. Anorg. Allg. Chem.* **1955**, *279*, 324-327.
(2) (a) Berul, S. I.; Lazarev, V. B.; Trippel, A. F.; Buchikhima, O. P. *Russ. J. Inorg. Chem.* **1980**, *25*, 1695-1697. (b) Trippel, A. F.; Lazarev, V. B.; Berul, S. I. *Russ. J. Inorg. Chem.* **1978**, *23*, 390-391.
(3) Kanishcheva, A. S.; Mikhailov, J. N.; Lazarev, V. B.; Trippel, A. F. *Dokl. Akad. Nauk, SSSR (Kryst.)* **1980**, *252*, 96-99.
(4) Schmitz, D.; Bronger, W. *Z. Naturforsch.* **1974**, *29b*, 438-439.
(5) Cordier, G.; Schafer, H.; Schwidetzky, C. *Rev. Chim. Miner.* **1985**, *22*, 676-683.
(6) Cordier, G.; Schafer, H.; Schwidetzky, C. *Rev. Chim. Miner.* **1985**, *22*, 631-638.
(7) (a) Feichtner, J. D.; Roland, G. W. *Appl. Opt.* **1972**, *11*, 993-998. (b) Ballman, A. A.; Byer, R. L.; Eimerl, D.; Feigelson, R. S.; Feldman, B. J.; Goldberg, L. S.; Menyuk, N.; Tang, C. L. *Appl. Opt.* **1987**, *26*, 224-227.
(8) Ibuki, S.; Yoschimatsu, S. *J. Phys. Soc. Jpn.* **1955**, *10*, 549-554.
(9) (a) Kaibe, H.; Tanaka, Y.; Sakata, M.; Nishida, I. *J. Phys. Chem. Solids* **1989**, *50*, 945-950. (b) Jeon, H.-W.; Ha, H.-P.; Hyun, D.-B.; Shim, J.-D. *J. Phys. Chem. Solids* **1991**, *4*, 579-585.
(10) (a) Smith, M. J.; Knight, R. J.; Spencer, C. W. *J. Appl. Phys.* **1962**, *33*, 2186-2190. (b) Testardi, L. R.; Bierly, J. N. Jr.; Donahoe, F. J. *J. Phys. Chem. Solids* **1962**, *23*, 1209. (c) Champness, C. H.; Chiang, P. T.; Parekh, P. *Can. J. Phys.* **1965**, *43*, 653-569. (d) Yim, W. M.; Fitzke, E. V. *J. Electrochem. Soc.* **1968**, *115*, 556-560.

0897-4756/93/2805-0331$04.00/0

thermal conductivity and are excellent materials for thermoelectric applications near room temperature.[11] With these properties in mind, we pursued the synthesis of new ternary alkali metal bismuth chalcogenide compounds using the now proven polychalcogenide flux method.[12,13] The latter involves the reaction of Bi in molten salts of A_2Q_x (A = alkali metal) of varying chemical composition.

We employed thermal analysis techniques to study the metal/alkali polychalcogenide flux reaction. Namely, differential scanning calorimetry (DSC) was used to monitor the various thermal events that occur during reaction and determine formation and crystallization of the products.

This paper describes the synthesis, structural characterization, optical and infrared spectroscopic, and charge transport properties of three new compounds, β-$CsBiS_2$, γ-$CsBiS_2$, and $K_2Bi_8Se_{13}$. The thermochemical characterization of the Bi/Cs_2S_x and Bi/K_2Se_x systems is also reported. The former two are new polymorphs of $CsBiS_2$ while the latter represents a new structure type.

Experimental Section

Reagents. Chemicals in this work were used as obtained: (i) bismuth powder, 99.999+% purity, -100 mesh; selenium powder, 99.5+% purity, -100 mesh, Aldrich Chemical Co., Inc., Milwaukee, WI; (ii) sulfur powder, sublimed, J. T. Baker Chemical Co., Phillipsburg, NJ; (iii) potassium metal, analytical reagent, Mallinckrodt Inc., Paris, KY; cesium metal, analytical reagent, Johnson Matthey/AESAR Group, Seabrook, NH (iv) methanol, anhydrous, Mallinckrodt Inc., Paris, KY; DMF, analytical reagent, diethyl ether, ACS anhydrous, EM Science, Inc., Gibbstown, NJ.

Synthesis. All manipulations were carried out under a dry nitrogen atmosphere in a Vacuum Atmospheres Dri-Lab glovebox. For the preparation of Cs_2S and K_2Se we used a modified literature procedure.[14]

Cesium Sulfide, Cs_2S. A 4.80-g (0.036 mol) sample of slightly heated (~30 °C) cesium metal was pipetted into a 250-mL round-bottom flask. A 150-mL volume of liquid ammonia was condensed into the flask at -78 °C (dry ice/acetone bath) under nitrogen to give a dark blue solution. Sulfur (0.579 g, 0.018 mol) and a Teflon-coated stirbar were added, and the mixture was stirred for 1 h to give a light blue solution. The NH_3 was removed by evaporation under a flow of nitrogen as the bath slowly warmed to room temperature. The pale yellow solid (97% yield) was dried in vacuum overnight, flame-dried, and ground to a fine powder with a mortar and pestle in the glovebox.

Potassium Selenide, K_2Se. A 10.098-g (0.128 mol) sample of selenium was combined with 10.00 g (0.256 mol) of freshly sliced potassium metal, and the reaction was carried out as above. The orange product (99% yield) was dried in vacuum overnight, flame-dried, and ground to a fine powder with a mortar and pestle in the glovebox.

β-Cesium Disulfidobismuthate(III), β-$CsBiS_2$ (I). Bi (0.052 g, 0.25 mmol), Cs_2S (0.335 g, 1.125 mmol), and S (0.064 g, 2.00 mmol) were mixed with a spatula in a glass vial. The mixture was transferred to a 6-mL Pyrex tube and was subsequently flame-sealed in vacuum (~10^{-3} Torr). The reaction was heated to 290 °C over a 12-h period in a computer controlled furnace, then isothermed at 290 °C for 96 hours, followed by cooling to 100 °C at a rate of 2 °C/hr, then to 50 °C in 1 h. This gave a red-orange glassy flux. The tube was opened with a glass cutter and the excess Cs_2S_x was dissolved in 150 mL of degassed methanol to give a clear, yellow solution. The insoluble product was washed with methanol repeatedly until the washings were colorless and then with ether. Transparent, dark, red needle-like crystals (0.085 g, 83% yield) were obtained along with a small amount of pale yellow impurity material. The red crystals and the amorphous yellow powder were insoluble in ethylenediamine, CH_3CN, DMF, ethanol, and CS_2. The mixture was quickly washed with 5 mL of water on a filter frit which removed the yellow impurity, followed by 20 mL of methanol. This final step was done quickly as the red crystals are slightly moisture sensitive. Prolonged exposure to water (several hours) resulted in the formation of a dark purple film on the surface of the crystals. Quantitative microprobe analysis on the red single crystals gave $Cs_{1.0}Bi_{1.0}S_{1.8}$ (average of four data acquisitions). It is important that the Cs_2S be made fresh using the method described here. Use of commercially available Cs_2S (e.g. Cerac Inc.) more often than not did not yield β-$CsBiS_2$ but resulted in Bi_2S_3. The difference in the two starting materials was examined using SEM. The particle size of the Cs_2S (Cerac) was considerably larger than that of Cs_2S (section 2.2), which could account for the difference in reactivities.

Reactions using increased amounts of starting materials generally yielded larger crystals. A mixture containing 0.105 g (0.500 mmol) of Bi, 0.670 g (2.25 mmol) of Cs_2S, and 0.128 g (4 mmol) of S under the same conditions afforded 3-mm-sized crystals suitable for single-crystal charge-transport studies.

γ-Cesium Disulfidobismuthate(III), γ-$CsBiS_2$. Bi (0.042 g, 0.20 mmol) Cs_2S (0.238 g, 0.80 mmol), and S (0.051 g, 1.60 mmol) were thoroughly mixed, and the reaction was carried out as above. The mixture was heated to 350 °C over a 12-h period and then isothermed for 6 days, followed by cooling to 80 °C at 2 °C/h and then to 50 °C in 1 h. The excess Cs_2S_x was removed by dissolving in degassed methanol. The product was then washed with ethyl ether (20 mL). Black hexagonal-shaped crystals (0.060 g, 74% yield) were obtained. Quantitative microprobe analysis gave $Cs_{1.0}Bi_{1.0}S_{2.2}$ (average of three acquisitions). Powder XRD peaks (d spacings, Å) 16.780 (vs), 12.468 (s), 8.268 (w), 6.267 (vw), 5.484 (w), 4.104 (vs), 3.592 (m), 3.410 (m), 3.314 (m), 3.231 (m), 3.025 (m), 2.927 (s), 2.868 (m), 2.730 (vw), 2.302 (vw), 2.266 (vw), 2.181 (vw), 2.150 (vw), 2.071 (m), 2.039 (m), 1.970 (vw), 1.909 (vw), 1.862 (vw), 1.813 (w), 1.761 (vw), 1.716 (vw), 1.634 (vw), 1.632 (vw).

Dipotassium Tridecaselenidooctabismuthate(III), $K_2Bi_8Se_{13}$ (II). Bi (0.209 g, 1.00 mmol), K_2Se (0.079 g, 0.500 mmol), and Se (0.316 g, 4.00 mmol) were thoroughly mixed, and the reaction was carried out as above. The mixture was heated to 330 °C over a 12-h period and then isothermed for 10 days, followed by cooling to 70 °C at 2 °C/h and then to 50 °C in 1 h. The excess K_2Se_x was removed by dissolving in degassed DMF. The product was washed with ether (20 mL) and ethylenediamine (20 mL) to remove any trace amounts of Se. Thin black needles with black microcrystalline powder (0.306 g, 88% yield) were obtained. Quantitative microprobe analysis gave $K_{2.0}Bi_{8.0}Se_{12.8}$ (average of four acquisitions).

The homogeneity of β-$CsBiS_2$ and $K_2Bi_8Se_{13}$ was confirmed by comparing the observed and calculated X-ray powder diffraction patterns. The d_{hkl} spacings observed for the bulk materials were compared, and found to be in good agreement with the d_{hkl} spacings calculated from the single crystal data using the program POWD10.[15] The results are summarized in Tables I and II.

Physical Measurements. *Infrared Spectroscopy.* FT-IR spectra of the β-$CsBiS_2$ compound were recorded as a solid in a CsI matrix. The sample was ground with dry CsI into a fine powder, and a pressure of about seven metric tons was applied to the mixture to make a translucent pellet. The spectra were recorded in the far-IR region (600–100 cm^{-1}, 4-cm^{-1} resolution) with the use of a Nicolet 740 FT-IR spectrometer equipped with a TGS/PE detector and silicon beam splitter.

Electron Microscopy. Quantitative microprobe analysis of the compounds was performed with a JEOL JSM-35C scanning

(11) (a) Rowe, D. M.; Bhandari, C. M. *Modern Thermoelectrics*; Holt, Rinehart and Winston: London, 1983; p 103. (b) Borkowski, K.; Przyluski, J. *J. Mater. Res. Bull.* **1987**, *22*, 381–387.

(12) (a) Kanatzidis, M. G. *Chem. Mater.* **1990**, *2*, 353–363. (b) Kanatzidis, M. G.; Park, Y. *J. Am. Chem. Soc.* **1989**, *111*, 3767–3769. (c) Kanatzidis, M. G.; Park, Y. *Chem. Mater.* **1990**, *2*, 99–101. (d) Park, Y.; Kanatzidis, M. G. *Angew. Chem., Int. Ed. Engl.* **1990**, *29*, 914–915.

(13) (a) Sunshine, S. A.; Kang, D.; Ibers, J. A. *J. Am. Chem. Soc.* **1987**, *109*, 6202–6204. (b) Kang, D.; Ibers, J. A. *Inorg. Chem.* **1989**, *27*, 549–551.

(14) Feher, F. *Handbuch der Praparativen Anorganischen Chemie*; Brauer, G., Ed.; Ferdinand Enke: Stuttgart, Germany, 1954; pp 280–281.

(15) Smith, D. K.; Nichols, M. C.; Zolensky, M. J. E. POWD10: "A Fortran IV Program for Calculating X-ray Powder Diffraction Patterns", version 10. Pennsylvania State University, 1983.

Table I. Calculated and Observed X-ray Powder Diffraction Patterns for β-$CsBiS_2$

$h\,k\,l$	d_{calcd}, Å	d_{obs}, Å	I/I_{max} (obs)
1 0 0	7.62	7.7	70
1 1 0	5.97	6.01	20
0 1 1	5.74	5.77	8
-1 1 1	5.01	5.03	4
1 1 1	4.25	4.25	20
1 2 0	4.06	4.07	18
0 2 1	3.99	3.99	36
-1 0 2, 2 1 0	3.542, 3.541	3.549	86
-2 1 1	3.45	3.46	46
1 2 1, 0 1 2	2.38, 2.36	3.36	21
-1 1 2	3.32	3.30	61
1 0 2	3.01	3.01	22
2 1 1, 1 3 0	2.95, 2.94	2.96	51
0 2 2, 1 1 2	2.872,2.870	2.869	61
-1 3 1, -2 1 2	2.812, 2.808	2.811	34
2 2 1	2.607	2.605	9
1 2 2	2.549	2.542	26
3 1 0, 2 3 0	2.455, 2.452	2.455	29
2 0 2	2.372	2.367	13
-3 0 2	2.315	2.331	14
-1 4 1	2.224	2.222	4
1 3 2	2.192	2.189	10
-1 2 3	2.168	2.167	18
1 4 1	2.143	2.147	17
2 2 2	2.127	2.127	19
1 1 3	2.101	2.100	23
-3 2 2, 3 2 1	2.085, 2.037	2.038	17
-3 3 1	2.005	1.993	7
4 0 0, 2 4 1	1.905, 1.900	1.908	100
4 1 0, 1 5 0	1.868, 1.864	1.874	28
-4 0 2	1.851		
-1 0 4	1.832	1.830	20
-4 2 1	1.803	1.806	17
1 3 3	1.787	1.785	9
-3 4 1	1.755	1.757	8
0 5 2, -1 5 2	1.694, 1.689	1.692	15
1 1 4, -2 4 3	1.643, 1.641	1.641	13
-3 1 4, 2 3 3	1.612, 1.605	1.606	6
-1 6 0, 0 3 4	1.578, 1.567	1.570	5

electron microscope (SEM) equipped with a Tracor Northern energy-dispersive spectroscopy (EDS) detector. Data were acquired using an accelerating voltage of 20 kV and a 1-min accumulation time. A 1.8 correction factor was applied to the Se atomic percent in this system as a result of examination of several other Se containing crystals.

UV/Vis/Near-IR Spectroscopy. Optical diffuse reflectance measurements were made at room temperature with a Shimadzu UV-3101PC double beam, double-monochromator spectrophotometer. The instrument was equipped with an integrating sphere and controlled by a personal computer. The measurement of diffuse reflectivity can be used to obtain values for the band gap which agree rather well with values obtained by absorption measurements from single crystals of the same material. The digitized spectra were processed using the Kaleidagraph software program. $BaSO_4$ powder was used as reference at all energies (100% reflectance). Absorption data were calculated from the reflectance data using the Kubelka–Munk function:[16]

$$\alpha/S = (1-R)^2/2R$$

R is the reflectance at a given wavelength, α is the absorption coefficient and S is the scattering coefficient. The scattering coefficient has been shown to be practically wavelength independent for particles larger than 5 μm which is smaller than the particle size of the samples used here.[16a,b] The bandgap was determined as the intersection point between the energy axis and the line extrapolated from the linear portion of the absorption edge in a $(\alpha/S)^2$ vs E plot.

Differential Scanning Calorimetry. Differential scanning calorimetry was performed with a computer-controlled Shimadzu

(16) (a) Wendlandt, W. W.; Hecht, H. G. *Reflectance Spectroscopy*; Interscience Publishers: New York, 1966. (b) Kotüm, G. *Reflectance Spectroscopy*; Springer-Verlag; New York, 1969. (c) Tandon, S. P.; Gupta, J. P. *Phys. Status Solidi* **1970**, *38*, 363–367.

Table II. Calculated and Observed X-ray Powder Diffraction Patterns for $K_2Bi_8Se_{13}$

$h\,k\,l$	d_{calcd}, Å	d_{obsd}, Å	I/I_{max} (obsd)
1 0 0	13.58		
0 1 0	12.08	12.4	11
1 1 0	9.20	9.33	8
-1 1 0	8.87		
-2 1 0	5.83	5.72	16
1 2 0	5.60		
3 0 0	4.53	4.56	13
1 3 0	3.90	3.99	11
1 -1 1, -2 1 1	3.595, 3.593	3.616	36
-3 2 0	3.56	3.58	33
-2 3 0	3.41	3.45	8
4 0 0, -1 2 1	3.40, 3.39	3.42	9
2 0 1, 4 1 0	3.31, 3.30	3.32	10
2 1 1, -3 -1 1	3.21, 3.20	3.23	45
0 4 0	3.02	3.08	5
-3 3 0	2.96	2.98	80
2 2 1	2.93	2.953	95
-3 -2 1	2.92	2.952	67
-4 2 0	2.89	2.85	5
2 4 0	2.80	2.80	10
3 -1 1	2.75	2.76	10
-5 1 0	2.63	2.63	4
2 -3 1	2.53	2.55	6
-3 4 0	2.472	2.490	11
-1 4 1, 0 -4 1	2.429, 2.428	2.451	35
4 -1 1	2.383	2.380	13
2 5 0	2.303	2.312	16
-2 5 0	2.251	2.278	8
2 -4 1	2.206	2.218	8
5 0 1, -6 0 1	2.125, 2.123	2.127	42
-1 0 2	2.081	2.083	100
5 4 0, 3 -4 1	2.057, 2.042	2.053	20
5 -2 1	1.985	1.986	16
2 6 0	1.950	1.948	18
-7 1 0	1.905	1.907	11
0 3 2	1.837	1.847	11
-2 -3 2	1.835	1.834	14
-1 6 1	1.805	1.798	15
-4 2 2	1.797	1.782	13
-5 -1 2	1.760	1.763	8
-4 6 0	1.705	1.728	11
2 -3 2	1.702	1.707	33
8 1 0	1.690	1.693	28
8 2 0	1.650	1.658	6
-7 4 0	1.607	1.629	9
0 7 1	1.595	1.607	8
2 -4 2	1.592	1.596	6
1 5 2	1.545	1.550	13

DSC-50 thermal analyzer under a nitrogen atmosphere at a flow rate of 35 mL/min. The appropriate reactant mixtures (~18.0 mg total mass), as mentioned above, were crimped in an aluminum pan inside a nitrogen-filled glovebox. The pan was placed on the sample side of the DSC-50 detector and an empty aluminum pan of equal mass was crimped and placed on the reference side. The samples were heated to the desired temperature at 3 °C/min and then isothermed for 800 min, followed by cooling at –0.5 °C/min to 75 °C. The reported DSC temperatures are peak temperatures with a standard deviation of 0.2 °C. The adopted convention in displaying data is exothermic peaks occur at positive heat flow while endothermic peaks occur at negative heat flow.

Charge-Transport Measurements. Dc electrical conductivity and thermopower measurements were made on single crystals and polycrystalline compactions of the compounds. Conductivity measurements were performed in the usual four-probe geometry with 60- and 25-μm diameter gold wires used for the current and voltage electrodes, respectively. Measurements of the sample cross-sectional area and voltage probe separation were made with a calibrated binocular microscope. Conductivity data were obtained with the computer-automated system described elsewhere.[17] Thermoelectric power measurements were made by using a slow ac technique[18] with 60-μm gold wires used to support and conduct heat to the sample, as well as to measure the voltage

(17) Lyding, J. W.; Marcy, H. O.; Marks, T. J.; Kannewurf, C. R. *IEEE Trans. Instrum. Meas.* **1988**, *37*, 76–80.

across the sample resulting from the applied temperature gradient. In both measurements, the gold electrodes were held in place on the sample with a conductive gold paste. Mounted samples were placed under vacuum (10^{-3} Torr) and heated to 320 K for 2–4 h to cure the gold contacts. For a variable-temperature run, data (conductivity or thermopower) were acquired during sample warming. The average temperature drift rate during an experiment was kept below 0.3 K/min. Multiple variable-temperature runs were carried out for each sample to ensure reproducibility and stability. At a given temperature, reproducibility was within ±5%.

Thermoelectric power results collected by the slow-ac technique require the production of a slowly varying periodic temperature gradient across the samples and measuring the resulting sample voltage. Samples were suspended between the quartz block heaters by 60-μm gold wires thermally grounded to the blocks with GE 7031 varnish. The magnitude of the applied temperature gradient was generally 1.0 K. Smaller temperature gradients gave essentially the same results but with somewhat lower sensitivity.

Crystallographic Studies. Both compounds were examined by X-ray powder diffraction for the purpose of phase purity and identification. Accurate d_{hkl} spacings (Å) were obtained from the powder patterns recorded on a calibrated (with FeOCl as internal standard) Phillips XRG-3000 computer-controlled powder diffractometer with Ni filtered Cu Kα radiation operating at 35 kV and 35 mA. The data were collected at a rate of 0.002°/s.

Structure Solution of β-$CsBiS_2$. A crystal with dimensions 0.50 × 0.20 × 0.10 mm was sealed in a glass capillary. Intensity data were collected using the ω–2θ scan mode on a Rigaku AFC6S four-circle automated diffractometer equipped with a graphite-crystal monochromator. The stability of the crystal was monitored by measuring three standard reflections periodically (every 150 reflections) during the course of data collection. No crystal decay was detected. An empirical absorption correction based on ψ scans was applied to the data, followed by a DIFABS correction to the isotropically refined data.[19] The structure was solved by direct methods using SHELXS86[20a] and refined by full-matrix least-squares techniques of the TEXSAN package of crystallographic programs.[20b] All calculations were performed on a VAXstation 3100/76 computer.

Structure Solution of $K_2Bi_8Se_{13}$. A crystal with dimensions 0.10 × 0.20 × 0.50 mm was mounted on a glass fiber. Intensity data for the crystal were collected using the $\omega/2\theta$ scan mode on a Rigaku AFC6S four-circle automated diffractometer. The stability of the crystal was monitored by measuring three standard reflections periodically (every 150 reflections) during the course of data collection. No crystal decay was detected. Absorption corrections were applied as above. The structure was solved by direct methods using SHELXS86 and refined by full-matrix least-squares techniques of the TEXSAN package of crystallographic programs. A careful inspection of the final structure revealed the presence of pseudo mirror symmetry perpendicular to the c axis. Since the α and γ angles of the unit cells are very close to 90°, we attempted to refine the model at the higher symmetry monoclinic space group $C2/m$ (No. 12) where $a' = 2a$, $b' = c$, $c' = -b$, $\beta = 87.96°$. The results where characterized by divergent refinement and an unstable structure. Thus, we chose the lower symmetry triclinic space group. All calculations were performed on a VAXstation 3100 Model 76 computer.

The complete data collection parameters, details of the structure solution and refinement and for both compounds are given in Table III. The coordinates and average temperature factors (B_{eq}) of all atoms and their estimated standard deviations for both compounds are given in Tables IV and V.

Table III. Summary of Crystallographic Data and Structure Analysis for β-$CsBiS_2$ and $K_2Bi_8Se_{13}$

	I	II
formula	β-$CsBiS_2$	$K_2Bi_8Se_{13}$
FW	406.01	2776.52
a, Å	7.794(5)	13.768(2)
b, Å	9.610(6)	12.096(3)
c, Å	7.329(4)	4.1656(6)
α, deg	90.000	89.98(1)
β, deg	102.16(5)	98.64(1)
γ, deg	90.000	87.96(1)
Z; V, Å^3	4; 537	1; 685
λ	0.710 73 (Mo Kα)	0.710 73 (Mo Kα)
space group	$P2_1/c$ (No. 14)	$P\bar{1}$ (No. 2)
D_{calc}, g/cm^3	5.03	6.73
μ, cm^{-1}	400 (Mo Kα)	684.2 (Mo Kα)
$2\theta_{max}$, deg	50 (Mo Kα)	50 (Mo Kα)
temp, °C	−36	23
final R/R_w, %	7.4/10	8.2/8.9
total data measured	1652	2443
total unique data	1551	2406
data with $F_o^2 > 3\sigma(F_o^2)$	1053	1171
no. of variables	38	107

Table IV. Fractional Atomic Coordinates and B_{eq} Values for β-$CsBiS_2$ with Estimated Standard Deviations in Parentheses

atom	x	y	z	B_{eq},[a] Å^2
Cs	−0.1383(4)	−0.4314(3)	−0.7879(4)	2.16(5)
Bi	0.4115(2)	−0.1657(2)	−0.1440(2)	1.48(2)
S1	0.186(1)	−0.256(1)	−0.461(1)	1.8(2)
S2	0.319(2)	0.084(1)	−0.199(2)	3.4(3)

[a] B values for anisotropically refined atoms are given in the form of the isotropic equivalent displacement parameters defined as $B_{eq} = {}^4/_3[a^2B(1,1) + b^2B(2,2) + c^2B(3,3) + ab(\cos\gamma)B(1,2) + ac(\cos\beta(1,3) + bc(\cos\alpha)B(2,3)$.

Table V. Fractional Atomic Coordinates and B_{eq} Values for $K_2Bi_8Se_{13}$ with Estimated Standard Deviations in Parentheses

atom	x	y	z	B_{eq},[a] Å^2
K	0.831(1)	0.051(2)	0.415(4)	2.6(8)
Bi1	0.8809(2)	0.3803(3)	0.4408(6)	1.6(1)
Bi2	0.3787(2)	0.5464(3)	1.1887(7)	1.6(1)
Bi3	1.1510(2)	0.2940(3)	0.0758(6)	1.6(1)
Bi4	0.5628(2)	0.8671(3)	0.2822(7)	1.8(1)
Se1	0.2625(5)	0.4267(7)	0.632(2)	1.6(3)
Se2	1.0370(5)	0.1977(7)	0.516(2)	1.7(3)
Se3	0.7788(5)	0.2707(7)	0.887(2)	1.7(3)
Se4	0.5094(5)	0.3536(7)	1.254(2)	1.6(3)
Se5	1.2811(5)	0.1169(7)	0.140(2)	1.5(3)
Se6	0.5837(5)	1.0886(7)	0.293(2)	1.4(3)
Se7	1.0000	0.5000	0.0000	1.2(4)

[a] B values for anisotropically refined atoms are given in the form of the isotropic equivalent displacement parameters defined as $B_{eq} = {}^4/_3a^2B(1,1) + b^2B(2,2) + c^2B(3,3) + ab(\cos\gamma)B(1,2) + ac(\cos\beta)B(1,3) + bc(\cos\alpha)B(2,3)$.

Results and Discussion

Synthesis and Spectroscopy. The synthesis of β-$CsBiS_2$ can be accomplished by dissolving Bi in a Cs_2S_x (x = 2.5–3.0) flux at 250–300 °C followed by isolation in degassed methanol. A direct combination reaction between Bi_2S_3 and Cs_2S (1:1) at 500 °C was performed to determine if the same compound could be isolated using this approach. The major product was found, by powder X-ray diffraction, to be β-$CsBiS_2$ but its morphology was microcrystalline. The advantage of the molten salt technique is the lower synthesis temperature and the larger size of obtained crystals suitable for comprehensive structural studies and property measurements. A number of microcrystalline A/Bi/S (A = alkali metal) phases have been synthesized, including α-$CsBiS_2$, via direct combination reactions of Bi_2S_3 and A_2S (A = alkali metal) at high temperatures (>500 °C), but no structural characterization is available.[21] To the best of our knowledge only the unit cell parameters of α-$CsBiS_2$ have been

(18) Marcy, H. O.; Marks, T. J.; Kannewurf, C. R. *IEEE Trans. Instrum. Meas.* **1990**, *39*, 756–760.
(19) Walker, N.; Stuart, D. *Acta Crystallogr.* **1983**, *A39*, 158–166.
(20) (a) Sheldrick, G. M. In *Crystallographic Computing* 3; Sheldrick, G. M., Kruger, C., Doddard, R., Eds.; Oxford University Press: Oxford, England, 1985; pp 175–189. (b) TEXSAN: Single Crystal Structure Analysis Software, Version 5.0 (1989). Molecular Structure Corp.: The Woodlands, TX 77381.

reported but no structural details have been found.[22]

Another new ternary phase, γ-$CsBiS_2$, was obtained by dissolving Bi in a Cs_2S_x (x = 3.0–3.7) flux at 350 °C. Stacks of black hexagonal plates were obtained from these reactions. SEM photographs showed a very thin platelike morphology for these crystals which made data collection difficult. A rhombohedral unit cell with a = 4.166(4) Å and c = 48.77(5) Å was found but the structure could not be refined to give a reasonable model. The unit cell of this compound is closely related to that of $RbBiS_2$[23] in which $CdCl_2$-type $(BiS_2)^-$ layers (perpendicular to the c axis) alternate with Rb^+ ions. The length of the c axis suggests six $(BiS_2)^-$ layers in the unit cell. The coordination sphere of Bi is perfect octahedral.

Similar investigations of Bi reactions in Li_2S_x and Na_2S_x (x = 2.2–5) fluxes in the temperature range 290–345 °C gave $LiBiS_2$ (68% yield) and $NaBiS_2$ (72% yield), which possess NaCl-type structures.[1a]

Far-IR spectroscopy of β-$CsBiS_2$ shows two absorptions at 286 cm^{-1} (s) and 226 cm^{-1} (m) which are similar to those of Bi_2S_3 at 290 cm^{-1} (w) and 220 cm^{-1} (s).[24] The two absorbancies are due to Bi–S stretching vibrations, but at this stage we cannot assign which modes since systematic IR spectroscopic data in this area are lacking. A solid-state far-IR of $K_2Bi_8Se_{13}$ shows no peaks, the only feature being a broad absorbance beginning at 200 cm^{-1}. The presence of this sort of feature is common in electrically conducting materials.

The synthesis of $K_2Bi_8Se_{13}$ can be accomplished by dissolving Bi in K_2Se_9 flux over a wide range of molar ratios at 330–370 °C followed by isolation in DMF. Similar investigations using Na_2Se_9 flux at 320 °C gave only $NaBiSe_2$[1c] along with a small amount of elemental Se, as confirmed by powder X-ray diffraction.

β-$CsBiS_2$ and $K_2Bi_8Se_{13}$ belong to the $(A_2Q)_n(Bi_2Q_3)_m$ (A = alkali metal; Q = S, Se) general family of compounds with n = 1 and m = 1, 4, respectively. Other members of this family include $CsBi_3S_5$ (n = 1, m = 3),[3] $Cs_3Bi_7Se_{12}$ (n = 3, m = 7),[5] and $K_2Bi_4S_7$ (n = 1, m = 2).[16] The latter phase has an unknown structure. The synthesis of other ternary bismuth chalcogenides with various n and m values may be possible, e.g., ABi_5Q_8 (n = 1, m = 5). Recently, another ternary bismuth sulfide $KBi_{6+x}S_{10}$ has also been synthesized which could belong to this family of compounds.[25]

Description of Structures. *Structure of β-$CsBiS_2$ (I).* This compound possesses the $CsSbS_2$ structure type.[26] The Bi lone pair is stereochemically active in this compound. The anion has a one-dimensional, polymeric structure with charge balancing Cs^+ cations found between the chains. Selected bond distances and angles for I are given in Table VI. The structure can be described as BiS_3 trigonal pyramids connected at two vertices to form fully extended $(BiS_2)_n^{n-}$ chains along the a axis. The two chains per unit cell are related by a center of symmetry. Figure 1 shows a view of an individual $(BiS_2)_n^{n-}$ chain. Along the chain backbone we can observe an alternation of long and short Bi–S1 bonds. Figure 2 shows two views of the unit cell along the a and b axes, respectively. The chains of β-$CsBiS_2$ are oriented in a sheetlike manner and the Bi lone pairs are directed into a nonpolar domain that is segregated from the polar domain of the Cs atoms. The $[BiS_2]^-$ framework can be thought of as a derivative of the well-known Bi_2S_3 compound and generated by successively dismantling the Bi_2S_3 framework by incorporation of Cs_2S.

Table VI. Selected Distances (Å) and Angles (deg) in the β-$CsBiS_2$ with Standard Deviations in Parentheses[a]

Bi–S1	2.531(9)	S1–Bi–S1′	88.1(3)
Bi–S1′	2.733(8)	S1–Bi–S2	100.3(4)
Bi–S2	2.505(9)	S1′–Bi–S2	93.5(3)
Bi–S2′	3.00(1)	S2–Bi–S2′	90.0(3)
Bi–S2″	3.52(1)	S1′–Bi–S2′	93.8(3)
		Bi–S1–Bi	99.0(3)
Cs–S1	3.533(9)	Bi–Bi′	3.909(3)
Cs–S2′	3.589(9)	Bi–Bi″	4.004(4)
Cs–S1″	3.54(1)		
Cs–S‴	3.598(9)		
Cs–S2′	3.64(1)		
Cs–S2″	4.13(1)		
Cs–S2‴	3.81(1)		
Cs–S(mean)	3.7(2)		

[a] The estimated standard deviations in the mean bond length and the mean bond angles are calculated by the equations $\sigma l = \{\sum_n (l_n - l)^2/n(n-l)\}^{1/2}$, where l_n is the length (or angle) of the nth bond, l the mean length (or angle), and n the number of bonds.

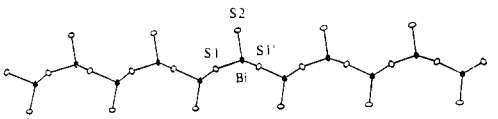

Figure 1. ORTEP representation of a single $(BiS_2)_n^{n-}$ chain with labeling scheme.

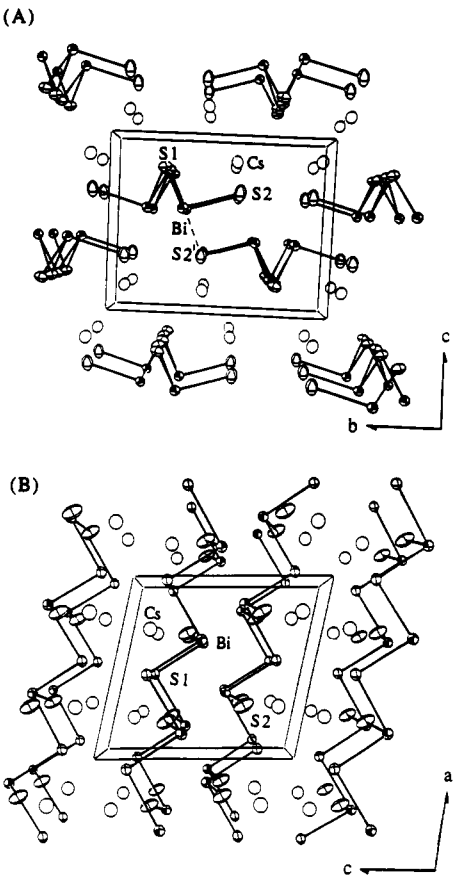

Figure 2. ORTEP packing diagrams of β-$CsBiS_2$ viewed along the a axis, (A) and b axis, (B). The shaded ellipsoids are Bi atoms, while open circles represent Cs atoms.

(21) Lazarev, V. B.; Trippel, A. F.; Berul, S. I. *Russ. J. Inorg. Chem.* **1980**, *25*, 1694–1697.
(22) Hoppe, R. *Bull. Soc. Chem. Fr.* **1965**, 1115–1121.
(23) Vorisholov, Y. V.; Peresh, E. Y.; Golovei, M. I. *Inorg. Mater.* **1972**, *8*, 677–678.
(24) Kagel, R. O.; Nyquist, R. A. *Infrared Spectra of Inorganic Compounds*; Academic Press: New York, 1971.
(25) Chen, L.-H.; McCarthy, T. J.; Kanatzidis, M. G., manuscript in preparation.
(26) Kanishcheva, A. S.; Mikhailov, Yu. N.; Kuznetsov, V. G.; Batog, V. N. *Dokl. Akad. Nauk SSSR* **1980**, *251*, 603–605.

Table VII. Selected Distances (Å) and Angles (deg) in the $[Bi_8Se_{13}]^{2-}$ Framework with Standard Deviations in Parentheses[a]

Bi1–Se1″	2.988(9)	Se1″–Bi1–Se2	175.9(3)
Bi1–Se2	3.009(8)	Se3–Bi1–Se7	176.4(2)
Bi1–Se3	2.847(9)	Se3′–Bi1–Se7′	176.1(2)
Bi1–Se3′	2.867(7)	Se1″–Bi1–Se3	92.88(2)
Bi1–Se7	3.038(3)	Se1″–Bi1–Se3′	92.6(2)
Bi1–Se7′	3.037(3)	Se1″–Bi1–Se7	88.3(2)
Bi1–Se (mean)	2.97(9)	Se1″–Bi1–Se7′	88.5(2)
		Se2–Bi1–Se3	90.3(2)
		Se2–Bi1–Se3′	89.9(2)
		Se2–Bi1–Se7	88.4(2)
		Se2–Bi1–Se7′	88.7(1)
		Se–Bi1–Se (mean)	90(2), 176.1(2)
Bi2–Se1	3.012(7)		
Bi2–Se1′	3.021(9)		
Bi2–Se3′	3.024(8)		
Bi2–Se4	2.881(8)		
Bi2–Se4′	2.869(9)		
Bi2–Se4″	2.878(7)		
Bi2–Se (mean)	2.95(7)		
Bi1–Se (mean)	2.97(9)	Se–Bi2–Se (mean)	90(3), 175(1)
Bi3–Se1	3.062(9)	Se1–Bi3–Se2	172.4(3)
Bi3–Se1′	3.067(7)	Se1′–Bi3–Se2′	172.3(3)
Bi3–Se2	2.860(9)	Se5–Bi3–Se7	179.9(2)
Bi3–Se2′	2.878(7)	Se–Bi3–Se (mean)	90(4), 175(4)
Bi3–Se5	2.730(8)		
Bi3–Se7	3.172(3)		
Bi3–Se (mean)	3.0(2)		
Bi4–Se4	3.552(8)	Se4–Bi4–Se4′	71.8(2)
Bi4–Se4′	3.551(9)	Se4–Bi4–Se6	141.9(2)
Bi4–$Se5_{eq}$	2.988(8)	Se4′–Bi4–Se6	141.8(2)
Bi4–$Se5'_{eq}$	2.987(7)		
Bi4–Se6	2.704(9)	Se5–Bi4–Se6	80.5(2)
Bi4–$Se6'_{eq}$	2.926(6)	Se5′–Bi4–Se6	80.5(2)
Bi4–$Se6''_{eq}$	2.913(7)	Se6′–Bi4–Se6	85.1(2)
Bi4–Se_{eq} (mean)	2.95(3)	Se6″–Bi4–Se6	85.0(3)
		Se–Bi4–Se6(mean)	83(2)

[a] The estimated standard deviations in the mean bond lengths and the mean bond angles are calculated by the equations $\sigma l = \{\sum_n (l_n - l)^2/n(n-l)\}^{1/2}$, where l_n is the length (or angle) of the nth bond, l the mean length (or angle), and n the number of bonds.

The S/Bi ratio increases from 1.50 to 2.00 upon going from Bi_2S_3 to $[BiS_2]^-$ as the structure is broken up into chains.

Since the shortest distance between chains is 3.00(1) Å, the structure can be alternatively viewed as layers of $(BiS_2)_n^{n-}$ chains separated with layers of Cs^+ ions. The terminal sulfur atoms in the chain are pointed toward the Cs^+ ions. The Bi–S bond distances in β-$CsBiS_2$ are comparable to those found in many bismuth sulfosalts, such as $PbCuBiS_3$.[27] Many of these sulfosalts have a fourth and fifth sulfur atom at greater distances from the Bi to form a square pyramidal coordination. In $KBiS_2$, the lone inert pair is not stereochemically active so the bismuth atom is found in a perfect octahedral environment with much longer Bi–S bonds at 3.02(1) Å.[1a] The same situation is thought to be present in γ-$CsBiS_2$. These longer bonds are due to the electrostatic repulsion between the lone pair around the Bi nucleus and the negatively charged S atoms.

The influence of the lone pair on Bi coordination is demonstrated through the inspection of the S–Bi–S angles, shown in Table VIII. This effect is consistent with predictions based on VSEPR theory.[28] The angles of β-$CsBiS_2$, in Table VI, are compared to the S–M–S angles found in the group 15 chainlike structures, $CsSbS_2$[26] and

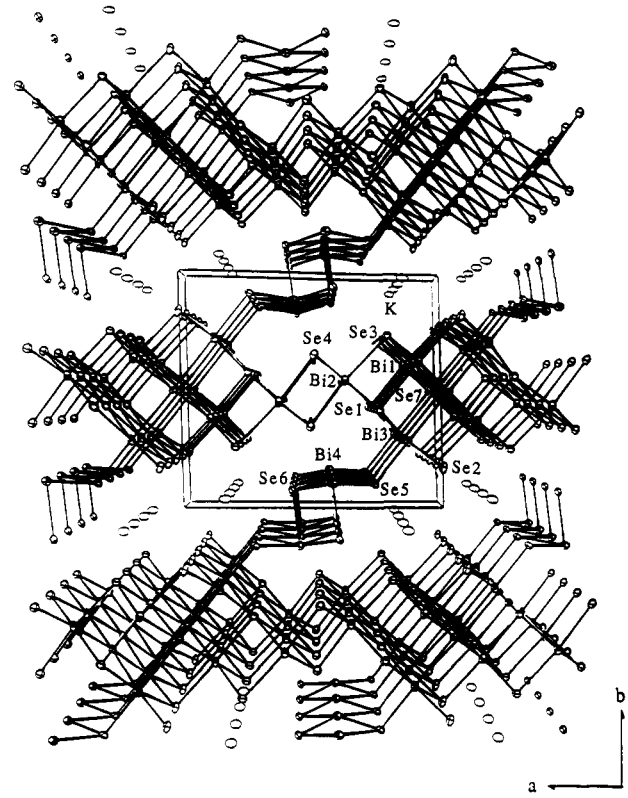

Figure 3. ORTEP representation of the packing diagram of $K_2Bi_8Se_{13}$ down the c axis. The shaded ellipsoids are the Bi atoms, and open ellipsoids are the K atoms.

Table VIII. Comparison of Bond Distances (Å) and Angles (deg) in Selected Group 15 Sulfides (M = As, Sb, Bi)

formula	S1–M–S1′	S1–M–S2	S1′–M–S2	M–S1	M–S2	M–S1′
$NaAsS_2$	95.5(1)	103.6(1)	102.0(1)	2.31(1)	2.17(1)	2.33(1)
$CsSbS_2$	89.06(5)	100.73(6)	95.28(6)	2.450(2)	2.366(2)	2.583(3)
β-$CsBiS_2$	88.1(3)	100.3(4)	93.5(3)	2.531(9)	2.505(9)	2.733(8)

$NaAsS_2$[29] (Table VIII). The angles decrease going from As to Bi, as the lone-pair orbital becomes larger and more diffuse. The long and short bond alternation along the chain (2.531(9) and 2.733(8) Å) and the short terminal bond of 2.505(9) Å are features that also appear in $CsSbS_2$ and $NaAsS_2$.

Structure of $K_2Bi_8Se_{13}$ (II). This compound has a complicated three-dimensional structure made up of $BiSe_6$ octahedra and $BiSe_5$ square pyramids, which form tunnels filled with K^+ cations. Selected bond distances and angles for II are given in Table VII.

The $BiSe_6$ octahedra form NaCl-type layers that are linked by $BiSe_5$ distorted square pyramids. Figure 3 shows the packing diagram of the extended structure down the c axis. The $[Bi_8Se_{13}]^{2-}$ framework can also be thought of as a hybrid of three different layered structure types interconnected to form a 3-D network. Structural features from the Bi_2Te_3,[30] Sb_2S_3,[31] and CdI_2[32] lattices are represented in this framework. Figure 4 shows the structures of the three layered materials (a–c). The features of the three structure types found in the $[Bi_8Se_{13}]^{2-}$ framework are highlighted in Figure 4d. The Bi_2Te_3-type fragments are linked by CdI_2-type octahedra to form sheets that are connected in the b direction by $BiSe_5$ square pyramids

(27) Kohatsu, I.; Wuensch, B. J. *Acta Crystallogr.* **1970**, *B27*, 1245–1252.
(28) (a) Gillespie, R. J. *Molecular Geometry*; Van Nostrand Reinhold: London, 1972; p 6. (b) Sawyer, J. F.; Gillespie, R. J. *Prog. Inorg. Chem.* **1987**, *34*, 65–113.
(29) Palazzi, M.; Jaulmes, S. *Acta Crystallogr.* **1977**, *B33*, 908–910.
(30) Villars, P.; Calvert, L. D. *Pearson's Handbook of Crystallographic Data for Intermetallic Phases*; American Society for Metals: Metals Park, OH, 1985; p 1494.
(31) Scavnicar S. *Z. Kristallogr.* **1960**, *114*, 85–97.
(32) Mitchell, R. S. *Z. Kristallogr.* **1956**, *108*, 296–315.

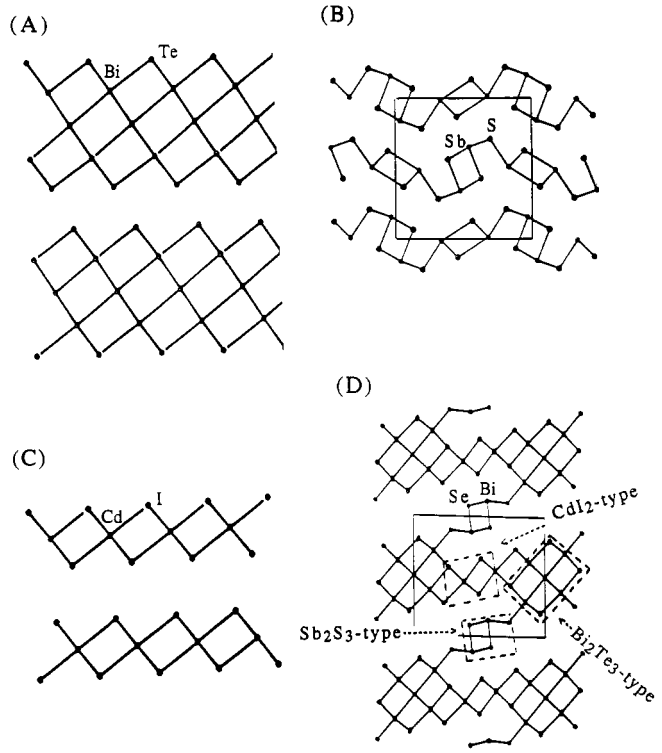

Figure 4. Projections of the structures of (A) Bi_2Se_3 (Bi_2Te_3-type), (B) Bi_2Se_3 (Sb_2S_3-type), (C) CdI_2-type, and (D) $[Bi_8Se_{13}]^{2-}$ framework. The three structure types found in this framework are designated with dashed lines.

(Sb_2S_3-type) to form the framework. Alternatively, the $[Bi_8Se_{13}]^{2-}$ framework can also be viewed as a derivative of the well-known Bi_2Se_3 compound generated by breaking down the Bi_2Se_3 framework by incorporation of K_2Se in the molar ratio of 4:1 (i.e., $[K_2Se][Bi_2Se_3]_4$). The Se/Bi ratio increases from 1.50 in Bi_2Se_3 to 1.63 for the $[Bi_8Se_{13}]^{2-}$ anion.

$K_2Bi_8Se_{13}$ is structurally related to $Cs_3Bi_7Se_{12}$[5] and $Sr_4Bi_6Se_{13}$.[6] In $Cs_3Bi_7Se_{12}$, the $[Bi_7Se_{12}]^{3-}$ anion is layered. It contains the CdI_2- and Bi_2Te_3-type fragments that were mentioned above but no Sb_2S_3 characteristics. The CdI_2-type octahedra link the Bi_2Te_3-type (or NaCl-type) blocks in an edge-sharing manner to form a lamellar structure. The highly charged $[Bi_6Se_{13}]^{8-}$ anion has a very interesting structure. It contains two-dimensional sheets made up of edge-sharing CdI_2- and Bi_2Te_3-type fragments. One-dimensional chains, comprised of Bi_2Te_3-type blocks, extend along the *b* direction and separate these layers.

Atoms Bi1 and Bi2 possess slightly distorted octahedral coordination as evidenced by the average bond distances and bond lengths in Table VII. The corresponding Bi–Se bond distances range from 2.847(9) Å to 3.038(3) Å for Bi1 and 2.869(9) Å to 3.021(9) Å for Bi2. These distances are similar to those reported for, $Cs_3Bi_7Se_{12}$.[5] The Bi3 coordination environment is distorted with a Bi3–Se5 bond distance of 2.730(8) Å which is trans to a long Bi3–Se7 distance of 3.172(3) Å. This same distorted coordination is found in $Cs_3Bi_7Se_{12}$.[5] This distorted octahedral coordination has been seen in several other bismuth compounds, including $Sr_4Bi_6Se_{13}$[6] and in several bismuth sulfosalts, including $PbBi_2S_4$ (galenobismuthite)[33] and $PbCu_4Bi_5S_{11}$.[34] Bi4 is the only atom in which the inert lone pair of electrons is stereochemically active as revealed

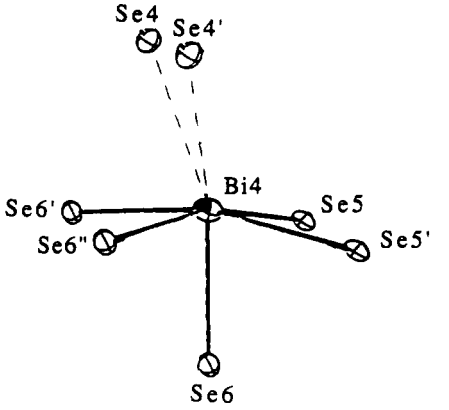

Figure 5. ORTEP representation of the Bi4 coordination in $K_2Bi_8Se_{13}$. Dashed lines designate long contacts.

by the distorted square pyramidal coordination shown in Figures 3 and 5. This coordination site consists of four equatorial bonds of 2.95(3) Å (ave) and a short axial distance of 2.704(9) Å. This short bond is trans to two Bi4–Se4 interactions at 3.552(1) (ave) which are shorter than the approximate sum of the van der Waals radii (4.4 Å).[35] The Se(4,4′)–Bi4–Se6 angles are much less than 180° at 141.8(2)° and 141.9(2)° and the Se6–Bi4–Se(6′,6″,5,5′) angles are less than 90° at 83(2)° (ave). This type of arrangement is found in the mixed metal compound, $Cu_{1.6}Bi_{4.8}Se_8$, where the Bi3 has a short axial bond of 2.71(1) Å that is trans to a Bi–Se distance of 3.54(1) Å with an angle of 139.4(4) Å.[36]

Thermal Analysis. Thermal analysis has been used previously to investigate the synthesis of solid-state compounds,[37] the mechanism of crystallization in chalcogenide glasses[38] and the high-temperature phase diagrams of many A_2Q/M_2Q_3 (A = alkali metal; Q = S, Se, Te; M = As, Sb, Bi) systems.[39] To study the reactions of Bi in the Cs_2S_x and K_2Se_x fluxes, we employed differential scanning calorimetry. The goal was to gain further insight into the thermal events that lead to the new compounds and the temperature at which they occur. The thermogram of a Bi/Cs_2S/*n*S mixture that leads to the synthesis of β-$CsBiS_2$ is given in Figure 6A and shows four exothermic peaks. To ascertain the origin of each peak, various control experiments were performed using Cs_2S/*n*S flux, Bi/Cs_2S and Bi/S mixtures under identical conditions. Analysis of the Cs_2S/S reaction thermogram shown in Figure 6B revealed two exothermic peaks (A, B) that are a result of atomic diffusion and reaction of Cs_2S with S to form a polysulfide flux. The flux reacts further with excess S to form a new polysulfide flux thereby producing exotherm C. Upon cooling, the excess flux solidifies at 178 °C (peak H). The same exothermic peaks are observed in the Bi/Cs_2S/*n*S mixture (Figure 6A) and thus are assigned to the same processes. The Cs_2S_x flux then reacts with Bi at 274 °C to produce β-$CsBiS_2$ giving rise to peak E in Figure 6. Endotherm D, at 270 °C, is assigned to the melting of Bi metal just prior to reaction with Cs_2S_x. All of the melted Bi immediately reacts at 274 °C (peak E), which is

(33) Iitaka, Y.; Nowacki, W. *Acta Crystallogr.* **1962**, *15*, 691–698.
(34) Kupcik, V.; Makovicky, E. *N. Jb. Miner. Mh.* **1968**, *7*, 236–237.
(35) Pauling, L. *The Nature of the Chemical Bond*, 3rd ed.; New York: Cornell University Press: Ithaca, NY, 1966; p 260.
(36) Liautard, B.; Garcia, J. C.; Brun, G.; Tedenac, J. C.; Maurin, M. *Eur. J. Solid State Inorg. Chem.* **1990**, *27*, 819–830.
(37) Wunderlich, B. *Thermal Analysis*; Academic Press: New York, 1990; pp 167–172.
(38) Hfiz, M. M.; Osman, M. A.; Abd El-Halim, A. S.; Abd El-Fadl, A. *Solid State Commun.* **1991**, *80*, 209–211.
(39) Berul, S. I.; Lazarev, V. B.; Trippel, A. F.; Buchikhina, O. P. *Russ. J. Inorg. Chem.* **1977**, *22*, 1390–1393.

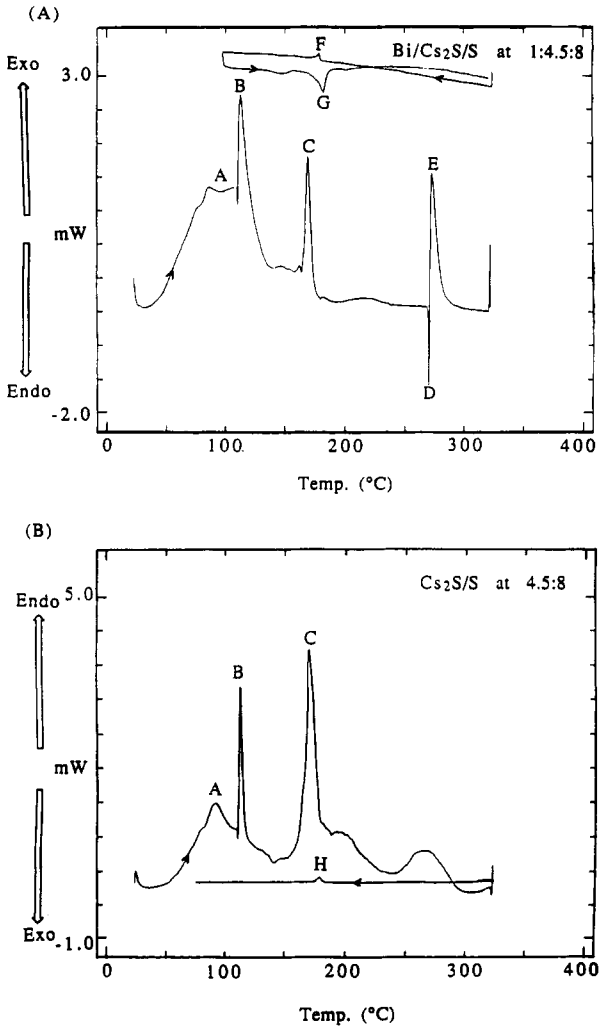

Figure 6. (A) DSC thermogram of the $Bi/Cs_2S_{2.8}$ mixture. The cooling and reheating curves are shown above the heating thermogram for clarity (peaks F and G). Peak temperatures (°C): A (97), B (113), C (170), D (270), E (274), F (176) and G (180). (B) DSC thermogram of the Cs_2S/S mixture. Peak temperatures (°C): A (92), B (112), C (170) and H (178).

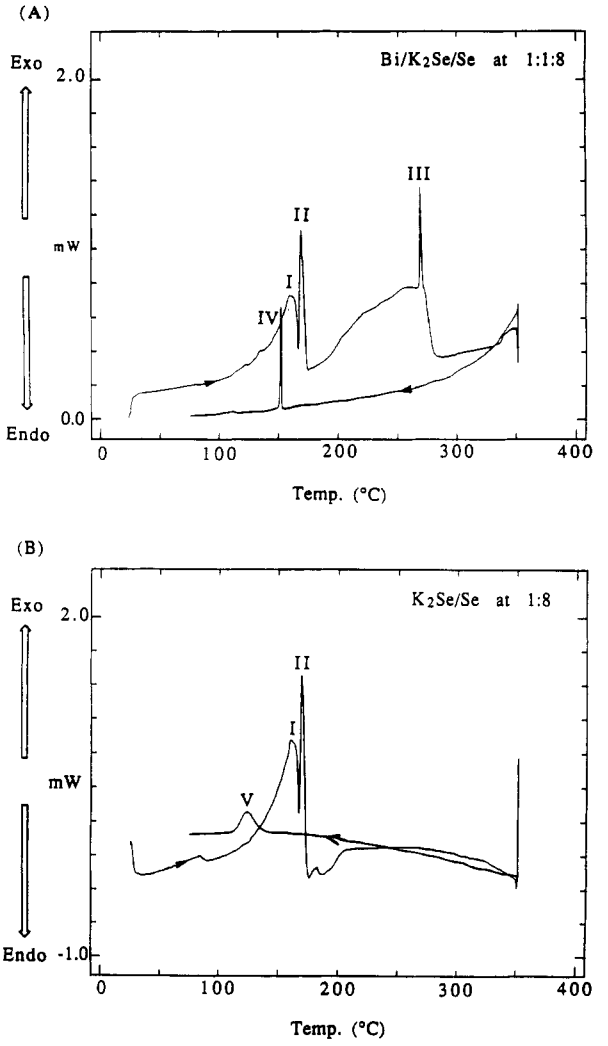

Figure 7. (A) DSC thermogram of the Bi/K_2Se_9 mixture. Peak temperatures (°C): I (160), II (169), III (269), and IV (152). (B) DSC thermogram of the K_2Se/Se mixture. Peak temperatures (°C): I (161), II (170), and V (123).

supported by the absence of a Bi recrystallization exotherm peak upon cooling. Peak E is assigned to the reaction of Bi and initial crystal nucleation. At 176 °C, exotherm F is observed on cooling which can be attributed to crystallization of the excess Cs_2S_x flux. A melting endotherm at 180 °C (peak G) was observed as the mixture was heated to 310 °C a second time. This result verified that peak F was due to excess flux crystallization and not due to product crystallization. To verify that peak F is not due to the crystallization of β-$CsBiS_2$, a bulk synthesis was carried out under the same heating and isotherm conditions in a sealed pyrex tube in a computer-controlled furnace. The reaction was quenched from 275 °C (after exotherm E) to room temperature. The product was isolated and powder XRD confirmed that the red crystals were single phase β-$CsBiS_2$.

It should be noted that Cs_2S purchased commercially yielded only Bi_2S_3, instead of β-$CsBiS_2$, under the conditions described here. This was confirmed with a bulk synthesis reaction in the furnace. Furthermore, DSC thermograms obtained from the Cs_2S/nS mixtures using this Cs_2S were completely different from that shown in Figure 6B. The small particle-size Cs_2S synthesized from the liquid ammonia method is very reactive and provides the best starting material for the synthesis of β-$CsBiS_2$. Care was taken to prevent any premature reaction at room temperature during the DSC experiments.

The thermogram for the synthesis of $K_2Bi_8Se_{13}$ is shown in Figure 7A. As in the β-$CsBiS_2$ synthesis described above, thermograms from K_2Se_x, Bi/K_2Se, and Bi/Se reactions were obtained for reference purposes. Clearly the exothermic peaks (I, II) are due to the reaction between K_2Se and Se to form a polyselenide flux as suggested by the control-reaction of K_2Se/Se whose DSC thermogram is given in Figure 7B. The redox reaction of Bi with the formed K_2Se_x flux occurs at 268 °C shown by the sharp exotherm III. However, the broad rise of the specific heat preceding peak III could also be attributed to product formation and reactant diffusion. DSC of the Bi + 8Se system produced a sharp endotherm at 226 °C corresponding to the melting of Se followed by a very sharp exotherm at 268 °C due to the formation of Bi_2Se_3. The formation of Bi_2Se_3 and $K_2Bi_8Se_{13}$ occurs at the approximate melting point of Bi metal which is masked in these systems. Exotherm IV in Figure 7A upon cooling, can be attributed to the crystallization of the excess K_2Se_x. Exotherm IV is at a different temperature than exotherm V (Figure 7B) because the excess K_2Se_x flux is of different chemical composition following the reaction with Bi metal. Bulk synthesis in the furnace at 330 °C, under DSC conditions, gave black needles of $K_2Bi_8Se_{13}$ upon quenching

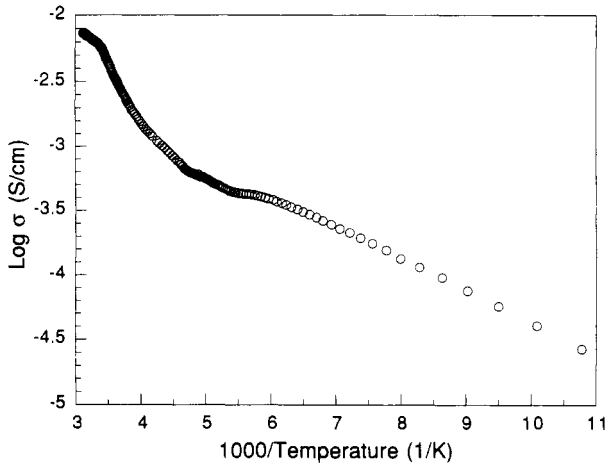

Figure 8. Variable temperature electrical conductivity data for a single crystal of γ-$CsBiS_2$.

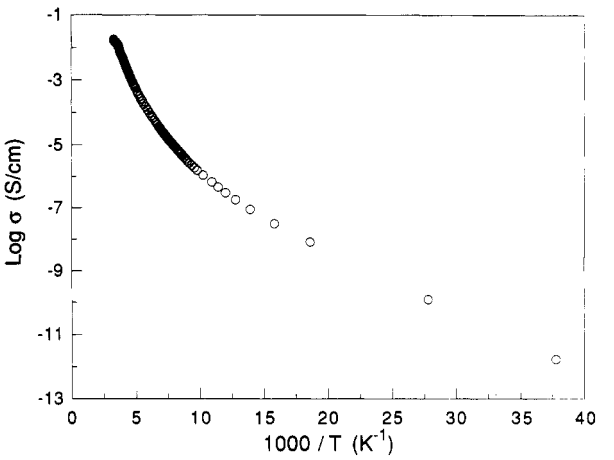

Figure 9. Variable temperature electrical conductivity data for pressed pellet of $K_2Bi_8Se_{13}$.

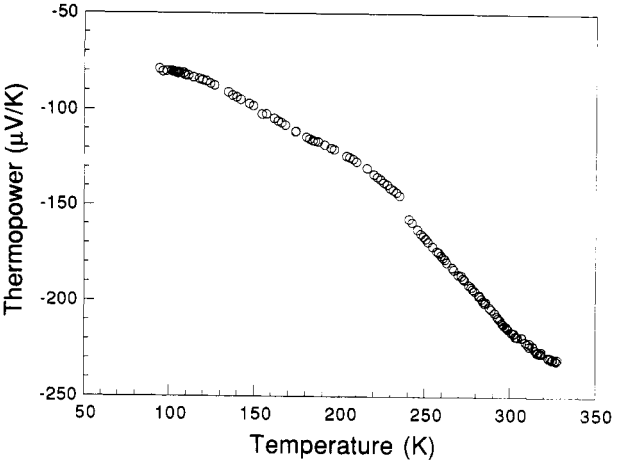

Figure 10. Thermoelectric power of a polycrystalline aggregate of $K_2Bi_8Se_{13}$ as a function of temperature.

from 275 °C to room temperature, supporting our assignment of exotherm IV.

As in β-$CsBiS_2$, crystal growth of $K_2Bi_8Se_{13}$ is not instantaneous, rather it is a gradual process which begins with nucleation at the reaction exotherm followed by growth at the heating and isotherm stages and briefly thereafter upon cooling. By studying these reactions with the DSC technique, we have identified the important reaction steps preceding the reaction of the metal with the flux and determined the exact reaction temperatures. On the basis of these results, we were able to reduce the total time of synthesis of these compounds from the original 10 days to only 24 h.

Electrical Conductivity and Thermoelectric Power Measurements. Four-probe electrical conductivity measurements on polycrystalline pellets of β-$CsBiS_2$ showed that the material is a semiconductor with room temperature conductivity $\sigma \sim 10^{-7}$ S/cm which drops rapidly to 10^{-12} S/cm for decreasing temperature. $K_2Bi_8Se_{13}$ is also a semiconductor but with enhanced charge transport as evidenced by both conductivity and thermoelectric power measurements as a function of temperature. In contrast, the room-temperature conductivity of single crystals of the layered γ-$CsBiS_2$ is $\sim 10^{-2}$ S/cm and exhibits a thermally activated temperature dependence, which is shown in Figure 8. Thermoelectric power data for γ-$CsBiS_2$ show a very large negative Seebeck coefficient (−580 μV/K at 120 K and −450 μV/K at 300 K) suggesting a *n*-type semiconductor. Figure 9 shows the log conductivity as a function of temperature for a pressed polycrystalline pellet of $K_2Bi_8Se_{13}$. This study was performed on two bulk samples of the compound with nearly identical results. The magnitude and temperature dependence of the conductivity suggest that the compound is a semiconductor. The conductivity of $\sim 10^{-2}$ S/cm at room temperature is compared to the values (1.6–2.0) × 10^3 S/cm for Bi_2Se_3 (Bi_2Te_3-type),[40] and 0.6–0.8 S/cm for Bi_2Se_3 (Bi_2S_3-type) obtained from single crystals of these materials.[41] The lower conductivity of $K_2Bi_8Se_{13}$ and the deviation from linearity particularly at low temperatures in the log σ vs $1/T$ plot (see Figure 9) may be due to the effects of grain boundaries in the pressed pellet. It should be noted that typically for three-dimensional materials the conductivities of polycrystalline compactions are 2–3 orders of magnitude lower than the corresponding values from single crystals. Efforts are continuing, to obtain larger single crystals that are suitable for conductivity measurements.

The conductivity measurements on polycrystalline pellets alone can not unequivocally characterize the electrical behavior of $K_2Bi_8Se_{13}$. A complementary probe to address this issue is thermoelectric power (TP) measurements as a function of temperature. TP measurements are typically far less susceptible to artifacts arising from the resistive domain boundaries in the material because they are essentially zero-current measurements. This is because temperature drops across such boundaries are much less significant than voltage drops. Figure 10 shows typical TP data of a polycrystalline aggregate of $K_2Bi_8Se_{13}$ as a function of temperature. The TP is negative throughout the temperature range studied ($80 < T < 300$ K) with values of −210 to −260 μV/K at room temperature. This indicates n-type charge transport. The TP becomes less negative as the temperature is decreased from 300 to 80 K, reminiscent of a metallike behavior, but the very large TP values suggest a semiconductor material. The semiconducting character of this material is also supported by the fact that an optical gap exists in this material in the near-IR region (vide infra). The room-temperature value of TP is comparable to that found in $Bi_2Te_{2.85}Se_{0.15}$,[9a] which is one of the best n-type thermoelectric materials available near room temperature. The high thermoelectric power at room temperature, coupled with the conductivity

(40) Black, J.; Conwell, E. M.; Seigle, L.; Spencer, C. W. *J. Phys. Chem. Solids*, **1957**, *2*, 240.

(41) Vereshchagin, L. F.; Itskevick, E. S.; Atabaeva, E. Y.; Popova, S. V. *Sov. Phys.-Solid State*, **1965**, *6*, 1763.

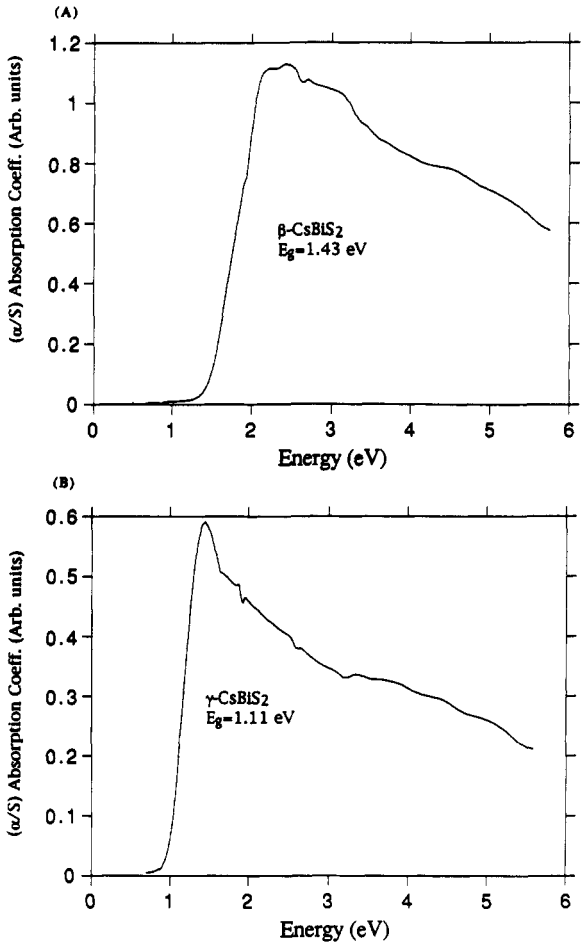

Figure 11. Top: Optical absorption spectrum of β-$CsBiS_2$. Bottom: Optical absorption spectrum of γ-$CsBiS_2$.

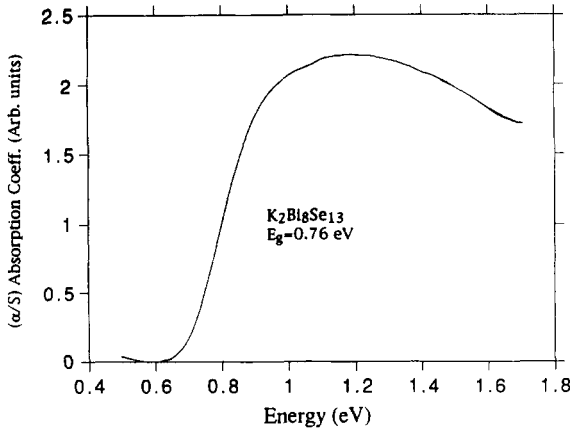

Figure 12. Optical absorption spectrum of $K_2Bi_8Se_{13}$. The absorption maximum occurs at 1.2 eV.

data suggest that γ-$CsBiS_2$ and $K_2Bi_8Se_{13}$ could be of interest as an n-type thermoelectric cooling materials.

UV–Visible–Near-IR Spectroscopy. The optical properties of β-$CsBiS_2$, γ-$CsBiS_2$, and $K_2Bi_8Se_{13}$ were assessed by studying the UV–visible–near-IR reflectance spectra of the materials. Such data for ternary bismuth chalcogenide compounds are reported here for the first time and thus comparisons with other materials are not possible. The spectra confirm the semiconductor nature of the materials by revealing the presence of optical gaps as shown in Figures 11 and 12. All compounds exhibit steep absorption edges from which the bandgap, E_g, can be assessed at 1.43, 1.11 and 0.76 eV for β-$CsBiS_2$, γ-$CsBiS_2$, and $K_2Bi_8Se_{13}$ respectively. The difference in band-gaps between the β- and γ-forms of $CsBiS_2$ is a direct consequence of the stereochemical expression of the s^2 lone pair of Bi which, in the two-dimensional γ-form, it is not stereochemically active. The smaller bandgaps of black $K_2Bi_8Se_{13}$ and γ-$CsBiS_2$ compared to the red β-$CsBiS_2$ are consistent with their respective colors. The bandgap order of $K_2Bi_8Se_{13}$, γ-$CsBiS_2$, and β-$CsBiS_2$ is also consistent with the decreasing order of electrical conductivity of these materials. A linear relationship is found in all compounds if the square of the absorption coefficient, $(\alpha/S)^2$, is plotted vs $(E - E_g)$, suggesting that the bandgaps are direct in nature.[42] However, independent confirmation is needed to verify this conclusion. By comparison, the corresponding bandgaps of Bi_2Se_3 and Bi_2S_3 are 0.35 and 1.3 eV, respectively.

Conclusions

The reaction of Bi with molten Cs_2S_x and K_2Se_x polychalcogenide fluxes has revealed three new bismuth phases, β-$CsBiS_2$, γ-$CsBiS_2$, and $K_2Bi_8Se_{13}$, respectively. β-$CsBiS_2$ and γ-$CsBiS_2$ are n-type semiconductors with optical bandgaps of 1.43 and 1.11 eV, respectively. $K_2Bi_8Se_{13}$ possesses a new structure type related to that of Bi_2Se_3. This compound is also an n-type semiconductor with a bandgap of 0.76 eV. At room temperature γ-$CsBiS_2$ and $K_2Bi_8Se_{13}$ show large negative thermoelectric power and relatively high conductivity.

Differential scanning calorimetry is a powerful technique in providing information on reactions of metals with polychalcogenide fluxes. We have been able to establish the region of product formation which helps to considerably shorten the reaction times. We hope to be able to use DSC to optimize the conditions of other molten salt reactions and reduce the time spent during the trial and error stage of exploratory synthesis.

Acknowledgment. Financial support from the National Science Foundation (DMR-9202428) is gratefully acknowledged. The X-ray instrumentation used in this work was purchased in part with funds from the National Science Foundation (CHE-8908088). The work made use of the SEM facilities of the Center for Electron Optics at Michigan State University. At Northwestern University this work made use of Central Facilities supported by NSF through the Materials Research Center (DMR-9190521).

Supplementary Material Available: Tables and atomic coordinates of all atoms and anisotropic and isotropic thermal parameters of all non-hydrogen atoms, bond distances, and angles (37 pages); a listing of calculated and observed ($10F_o/10F_c$) structure factors (36 pages). Ordering information is given on any current masthead page.

(42) Pankove, J. I. In *Optical Processes in Semiconductors*, Dover Publications: New York, 1975.